Earth and Planetary Science Letters 427 (2015) 202–214

Contents lists available at ScienceDirect

Earth and Planetary Science Letters

www.elsevier.com/locate/epsl

Hydrous basalt–limestone interaction at crustal conditions: Implications for generation of ultracalcic melts and outflux of CO_2 at volcanic arcs

Laura B. Carter *, Rajdeep Dasgupta

Dept of Earth Science, Rice University, 6100 Main St, MS-126, Houston, TX 77005, USA

ARTICLE INFO

Article history:
Received 29 January 2015
Received in revised form 22 June 2015
Accepted 25 June 2015
Available online 24 July 2015
Editor: J. Brodholt

Keywords:
experimental petrology
limestone assimilation
CO_2 degassing
arc volcanism
ultracalcic melt inclusions

ABSTRACT

High degassing rates for some volcanoes, typically in continental arcs, (e.g., Colli Albani Volcanic District, Etna, Vesuvius, Italy; Merapi, Indonesia; Popocatepetl, Mexico) are thought to be influenced by magma–carbonate interaction in the crust. In order to constrain the nature of reaction and extent of carbonate breakdown, we simulated basalt–limestone wall-rock interactions at 0.5–1.0 GPa, 1100–1200 °C using a piston cylinder and equal mass fractions of calcite ($CaCO_3$) and a hydrous (~4 wt.% H_2O) basalt in a layered geometry contained in AuPd capsules. All experiments produce melt + fluid + calcite ± clinopyroxene ± plagioclase ± calcic-scapolite ± spinel. With increasing T, plagioclase is progressively replaced by scapolite, clinopyroxene becomes CaTs-rich, and fluid proportion, as inferred from vesicle population, increases. At 1.0 GPa, 1200 °C our hydrous basalt is superliquidus, whereas in the presence of calcite, the experiment produces calcite + clinopyroxene + scapolite + melt. With the consumption of calcite with increasing T and decreasing P, melt, on a volatile-free basis, becomes silica-poor (58.1 wt.% at 1.0 GPa, 1100 °C to 34.9 wt.% at 0.5 GPa, 1200 °C) and CaO-rich (6.7 wt.% at 1.0 GPa, 1100 °C to 43.7 wt.% at 0.5 GPa, 1200 °C), whereas Al_2O_3 drops (e.g., 19.7 at 1100 °C to 12.8 wt.% at 1200 °C at 1.0 GPa) as clinopyroxene becomes more CaTs-rich. High T or low P melt compositions are 'ultracalcic,' potentially presenting a new hypothesis for the origin of ultracalcic melt inclusions in arc lava olivines. Wall-rock calcite consumption is observed to increase with increasing T and decreasing P. At 0.5 GPa, our experiments yield carbonate assimilation from 21.6 to 47.6% between 1100 and 1200 °C. Using measured CO_2 outflux rates for Mts. Vesuvius, Merapi, Etna and Popocatepetl over a T variation of 1100 to 1200 °C at 0.5 GPa, we calculate 6–92% of magmatic input estimates undergo this extent of assimilation, suggesting that up to ~3% of the current global arc CO_2 flux may be crustally derived. Application of the assimilation extent bracketed in this study to the estimated elevated number of carbonate-assimilating arc magmatic systems active during the late Cretaceous to early Paleogene suggests that magma-induced upper plate decarbonation alone had the potential to contribute up to 2.7×10^{14}–5.6×10^{15} g/y CO_2, assuming no dilution and complete gaseous release of all assimilated carbon. Using an estimated assimilation extent averaged from current systems gives a slightly lower though still significant value of $\leq 5.5 \times 10^{14}$ g/y of excess CO_2 being released into the atmosphere.

1. Introduction

Carbon dioxide released through arc volcanoes is conventionally assumed to be mantle-derived with an input from the subducted slab, and a range of carbon transfer mechanisms from the downgoing slab to the overlying mantle wedge has been proposed (e.g., Behn et al., 2011; Dasgupta et al., 2013; Duncan and Dasgupta, 2014, 2015; Shaw et al., 2003; Skora et al., 2015; Tsuno and Dasgupta, 2012; Tsuno et al., 2012). Although this may be dominant for most arc volcanoes situated on oceanic crust, i.e., for island arcs, the scenarios for volcanic degassing of CO_2 may be vastly different in arc volcanoes underlain by significant carbonate strata (e.g., Lee et al., 2013). For example, anomalously high CO_2 degassing rates currently estimated at several continental arc volcanoes (e.g., Burton et al., 2013; Caliro et al., 2005; Frondini et al., 2004) are thought to be augmented by carbonates in the up-

* Corresponding author. Tel.: +1 713 348 5087.
E-mail addresses: Laura.B.Carter@rice.edu (L.B. Carter), Rajdeep.Dasgupta@rice.edu (R. Dasgupta).

http://dx.doi.org/10.1016/j.epsl.2015.06.053
0012-821X/

per plate. Carbonate assimilation is identified in natural systems not only by heightened emissions, but also by: the presence of skarn xenoliths (e.g., Barnes et al., 2005; Di Rocco et al., 2012; Goff et al., 2001); carbon, strontium, and neodymium isotopes, which can become contaminated with crustal signatures (Barnes et al., 2005; Chadwick et al., 2007; Troll et al., 2012), though sometimes clear evidence is lacking (Halldórsson et al., 2013); and calcium-rich mineralogy typical of endoskarns (Di Rocco et al., 2012; Einaudi and Burt, 1982; Kerrick, 1977). Magma–carbonate interactions are also reflected in compositions of glasses and melt inclusions that become uniquely silica-undersaturated and calcium-enriched (Watkinson and Wyllie, 1964).

The lines of evidence in support of active crustal carbonate assimilation by magmas, predominantly expelled at arc volcanoes, have been well-documented in the field at Mount Merapi, Indonesia (Chadwick et al., 2007; Deegan et al., 2010; Troll et al., 2012); Popocatepetl, Mexico (Goff et al., 2001 and references therein); Pacaya, Guatemala (Goff et al., 2001); Santorini and Nisyros, Greece (Spandler et al., 2012); Etna, Italy (Michaud, 1995); Vesuvius, Italy (Iacono-Marziano et al., 2009, 2008; Jolis et al., 2013); and the Colli Albani Volcanic District (CAVD[1]) in Italy's Roman Province (Di Rocco et al., 2012; Freda et al., 2008; Gaeta et al., 2009; Iacono-Marziano et al., 2007; Mollo and Vona, 2014; Mollo et al., 2010). Decarbonation amplifies the outgassing efficiency in these systems by the general reaction:

$$CaCO_3\ (\text{solid}) \rightarrow CaO\ (\text{melt}) + CO_2\ (\text{gas}) \quad (1)$$

which has the potential to increase explosivity at the vent (e.g., Troll et al., 2012).

Previous experimental studies simulated the natural systems of Italy (Conte et al., 2009; Iacono-Marziano et al., 2009, 2008, 2007; Jolis et al., 2013; Mollo et al., 2010) and central Java, Indonesia (Deegan et al., 2010). Two studies utilized Indonesian and Vesuvian samples in time-series disequilibrium experiments, which determined that the rapidity of the reaction is exceedingly fast (Deegan et al., 2010; Jolis et al., 2013). Using estimated temperatures and pressures of limestone–magma interaction scenarios (e.g., 3–15 km, Roman Province, Freda et al., 1997; 10–15 km, Merapi, Troll et al., 2012), previous experiments kept pressure constant (at $\leq$0.5 GPa) with or without a minor temperature range. Water content and crustal input was varied, though the mass fraction of carbonate added to experiments was limited to $<$20 wt.%, simulating perhaps a stoped interaction with a limited availability of carbonate. The goal was focused either on using a carbonate quantity that reproduced results matching natural systems, or on following the liquid line of descent (Conte et al., 2009; Freda et al., 2008; Iacono-Marziano et al., 2007). Only some of the experiments discerned pressure–temperature effects (Freda et al., 2008; Iacono-Marziano et al., 2008), but remained at very low pressures ($\leq$0.5 GPa) while underthrusted carbonates in e.g., the cretaceous, could have been assimilated at up to 30 km depth (e.g., DeCelles et al., 2009; Lackey et al., 2005).

This study fills the lack in data regarding the effect of pressure (depth within the crust) and temperature (extent of basaltic crystallization, discerned by calcite-free experiments) on limestone–basalt interaction, with conditions astride the basaltic liquidus at mid- to lower-crustal depths, such that results may be applicable to calcite assimilation conditions of various present and past volcanic systems. Furthermore, we simulate the reactive front that forms in natural systems between an intruding magma body and a carbonate wall-rock by layering an excess of pure limestone with typical near-primary arc basalt. We determine residual mineralogy and melt compositions as a function of reactive crystallization, pressure, and temperature. Our data have implications for ultra-calcic melt inclusions that have been identified in subduction-zone settings and constrain the extent of assimilation and the maximum limit of excess magmatic CO_2 that may be derived from upper plate magma–limestone interactions as a function of depth and temperature.

2. Methods

2.1. Starting materials

To represent the intruding magma, a synthetic primary arc basalt (MgO ~6.2 wt.%) was used, similar in composition to natural Strombollian K-basalt used by Iacono-Marziano et al. (2007) and natural Vesuvian shoshonite in the experiments of Jolis et al. (2013), though a characteristic of Italian lavas is an elevated potassium content not reproduced in this study (Supplementary Table 1). Reagent grade oxides and carbonates were first dried by firing SiO_2, TiO_2, Al_2O_3 and MgO overnight at 1000 °C, Fe_2O_3 at 800 °C, MnO_2 at 400 °C, $CaCO_3$ at 250 °C, and K_2CO_3 and Na_2CO_3 at 110 °C. Using a microbalance, these powders were measured out to predetermined portions to generate the basaltic composition desired and combined. The mixture was then ground to a powder and homogenized in an agate mortar under ethanol, after which the ethanol was evaporated off. To reduce the Fe_2O_3 to FeO and drive off CO_2, the mixture was heated to 1000 °C in a CO–CO_2 gas mixing furnace at log fO_2 ~ FMQ-2 for 24 h. Finally, gibbsite [$Al(OH)_3$] was added, contributing 4.03 wt.% water to the hydrous melt and bringing the alumina content up to the desired level. The second starting material representing the intruded crustal carbonate was pure $CaCO_3$ powder. Both starting materials were stored covered at 110 °C to minimize water adsorption.

2.2. Experimental methods

Experiments were performed in a 1/2-inch end-loaded piston cylinder apparatus at Rice University following the standard protocol detailed in Tsuno and Dasgupta (2011). Starting materials were packed in coned $Au_{75}Pd_{25}$ capsules in a layered geometry with calcite underlying synthetic basalt, in a 1:1 ratio by weight (with error $\leq$0.1 wt.%). Capsules were weighed before and after being line-welded shut to ensure that volatile loss was negligible. To consider a range of pressures and temperatures relevant for lower- to mid-crustal intrusions, experiments were conducted at three distinct pressures of 0.5 GPa (~15 km deep), 0.8 GPa, and 1.0 GPa (~35 km deep) and between 1100 and 1200 °C (Table 1). An additional set of calcite-free experiments were also performed at 1.0 GPa to determine the phase compositional evolution along the liquid line of descent of the starting basalt uncontaminated by calcite. Run duration ranged from 3 to 72 h. Initially, the recovered capsules were ground until the edge of the sample was visible before being impregnated with epoxy to prevent sample loss. Final polish was achieved using dry polycrystalline diamond powder (3, 1, 0.25 μm) on nylon and velvet surfaces.

2.3. Analytical techniques

Polished samples were carbon-coated and studied for phase identification and major element phase composition using a Cameca SX100 electron microprobe at NASA Johnson Space Center in Houston, Texas. Analysis was performed using a 15 kV, 10 nA electron beam with spot sizes varied between 10 μm on calcite and glass and a focused 1 μm on silicate grains and smaller melt pools. Peak counting times for Si, Al, Ti, Fe, Mn, and Mg were

[1] **Abbreviations:** P = pressure, T = temperature, X = composition, F = melt fraction, CAVD = Colli Albani Volcanic District.

Table 1
Experimental run conditions, phase assemblages, estimated phase proportions, and extent of CO_2 released.

Run no.	P (GPa)	T (°C)	Duration (h)	Run products (wt.%)[a]								Released CO_2[b]
				Opx	Sp	Plag	Sc	Cpx	Cc	Melt	$\sum r^2$	
Calcite-free, hydrous basalt												
B252	1.0	1100	24	6.7	3.4	38.7	–	35.5	–	15.7	0.3	–
B291	1.0	1150	24	–	7.2	22.7	–	38.4	–	31.7	1.0	–
B294	1.0	1175	24	–	6.2	9.5	–	21.0	–	63.3	0.7	–
B262*	1.0	1200	24	–	–	–	–	–	–	100.0	–	–
50 wt.% $CaCO_3$, 50 wt.% hydrous basalt (layered)												
B292	1.0	1100	72	–	2.3	21.1	–	28.3	48.3	0.0	0.1	0.8
B306	1.0	1150	48	–	2.8	15.2	0.0	23.7	49.6	8.7	0.1	0.2
B293	1.0	1175	24	–	–	–	2.6	38.1	41.3	18.0	0.8	3.8
B263*	1.0	1200	24	–	–	–	0.0	34.3	40.2	25.5	0.6	4.3
B274	0.8	1100	72	–	2.5	18.6	–	32.6	46.3	0.0	0.8	1.6
B297	0.8	1125	48	–	2.1	11.3	0.0	27.6	47.8	11.2	0.0	1.0
B264	0.8	1150	24	–	1.3	2.1	0.0	30.4	40.0	26.2	0.2	4.4
B283	0.8	1175	24	–	4.3	1.6	0.0	20.2	49.2	24.7	0.1	0.4
B266	0.8	1200	24	–	2.0	–	0.0	21.7	36.7	39.6	0.5	5.8
B267*	0.5	1100	48	–	0.0	6.7	–	31.6	39.2	22.5	0.5	4.8
B295	0.5	1125	24	–	3.7	0.0	0.0	28.0	33.8	34.5	0.4	7.1
B298	0.5	1150	24	–	4.8	0.0	0.0	23.6	28.6	43.0	0.5	9.4
B280[c]	0.5	1175	>16	–	2.7	–	–	10.9	31.3	55.1	0.2	8.2
B279*	0.5	1200	24	–	4.9	–	–	–	26.2	68.9	0.3	10.5

[a] Run products are given as modal proportion as calculated by mass balance on a volatile-free basis (see Methods).
[b] Released CO_2, also in wt.%, is calculated stoichiometrically from calcite consumed (50-Cc, in wt.%) indicating the estimated proportion of CO_2 released to melt + vapor.
Phases with "–" were not identified in the product, whereas a value of 0.0 was present but in trace amounts; Opx = orthopyroxene, Sp = spinel, Plag = plagioclase, Sc = scapolite, Cpx = clinopyroxene, Cc = calcite, melt = silicate melt; $\sum r^2$ is the sum of residual squares after mass balance fit between run products and initial starting composition.
[c] Run no. B280 quenched before the planned 24 h run duration, but texturally and chemically appears to have approached equilibrium.
For runs indicated with $^*fO_2$ was determined: B262* = ΔFMQ + 1.4 ± 0.3 or 2.4 ± 0.3; B263* = ΔFMQ + 1.8 ± 0.2 or 2.8 ± 0.1 (using the models of Barr and Grove, 2010 or Balta et al., 2011, respectively); B267* = ΔFMQ − 0.30 ± 0.1; B279* = ΔFMQ + 0.41 ± 0.1 (using the T-dependent model of Barr and Grove, 2010).

30 s with 10 s background counts, whereas 20 s peak counting time, with 10 s background, was used for K and Na, both of which were analyzed first on their respective spectrometer to minimize volatility-induced loss. Standards used were a combination of natural minerals and synthetic glasses. Multiple spot analyses (n) were performed for each phase. Location was considered within and away from the reaction front between the basalt and carbonate layers; line analyses were taken for samples containing large melt pools. Analyses of the AuPd capsule adjacent to the melt pool were also performed using Fe, Au, and Pd metal standards to estimate the oxygen fugacity prevailing during the experiments (see Supplementary information).

Little variation of phase compositions away from the reaction front, an absence of a chemically-distinctive rim on residual minerals (e.g., clinopyroxene), and low mass balance residuals obtained using average phase compositions across the entire charge (Table 1), confirm that experiments approached equilibrium and maintained closed system.

Mass proportions of phases present were calculated using volatile-free-normalized compositions based on a least square minimization approach. Calcite consumption was estimated by subtracting the modal proportion of remaining calcite determined by mass balance calculations from the starting fraction in the system (0.50). Carbonate assimilation was then determined as the percentage of calcite consumed per unit mass of basaltic melt. Estimation of the CO_2 budget of the fluid plus melt was made with the estimate of consumed calcite.

3. Results

3.1. Texture and phase assemblage

Fig. 1 shows the texture of the experimental products and Fig. 2 shows the phase assemblages obtained from the experiments in P–T space. Modal proportions, calculated by mass balance on a volatile-free basis, are given in Table 1 and plotted as a function of temperature in Fig. 3.

All experiments produce melt and mineral phases including ± clinopyroxene ± spinel ± plagioclase ± orthopyroxene (in calcite-free experiments only) ± scapolite (in calcite-bearing experiments only) (Table 1, Figs. 1, 2, 3). Calcite–basalt reaction experiments contain crystalline calcium carbonate, silicate glass, and circular void spaces, which are interpreted as an equilibrium CO_2-rich fluid phase present during the experiments. Owing to the initial layered arrangement of the starting materials in basalt–calcite experiments, the resulting phases tend to be oriented with vapor and melt at the top (particularly when melt fraction is substantial enough to interconnect, i.e., $F > \sim 0.1$, similar to calcite-free melt location), an interaction front containing the majority of crystalline silicate phases, when present, in the middle, and remnant calcite at the bottom (Fig. 1). Mineral phases forming at the reaction front are for the most part clinopyroxene, in addition to plagioclase at low temperatures and/or scapolite in intermediate to hotter conditions. Plagioclase forms only at low temperatures at all pressures (Table 1, Fig. 2) as small tabular to lathe-like crystals, though near exhaustion it occurs in such small quantities, generally confined to rims around clinopyroxene crystals (Fig. 1). In the presence of calcite, plagioclase disappears at temperatures ≥1150 °C at 0.5 GPa, less sharply at 0.8 GPa where it gradually diminishes between 1125 and <1200 °C as scapolite fades in, and >1175 °C at 1.0 GPa (Fig. 2). Anhedral to subhedral hexagons of scapolite (Fig. 1) appear at intermediate temperatures at all pressures (Table 1) with the breakdown of plagioclase and calcite. At higher pressures, the gradual replacement of plagioclase by scapolite coincides with an increase in melt fraction, F ($F = 0.07$ at 1150 °C; $F = 0.30$ at 1175 °C, 1.0 GPa) and calcite consumption. This shift occurs at lower temperatures with decreasing pressure (1125 ± 25°C at 0.8 GPa; <1100 °C, 0.5 GPa). Clinopyroxene is present as sub- to euhedral prismatic grains at nearly all conditions, only absent at low pressure and high temperature (0.5 GPa, >1175 °C; Fig. 1) in calcite-bearing experiments. Small proportions

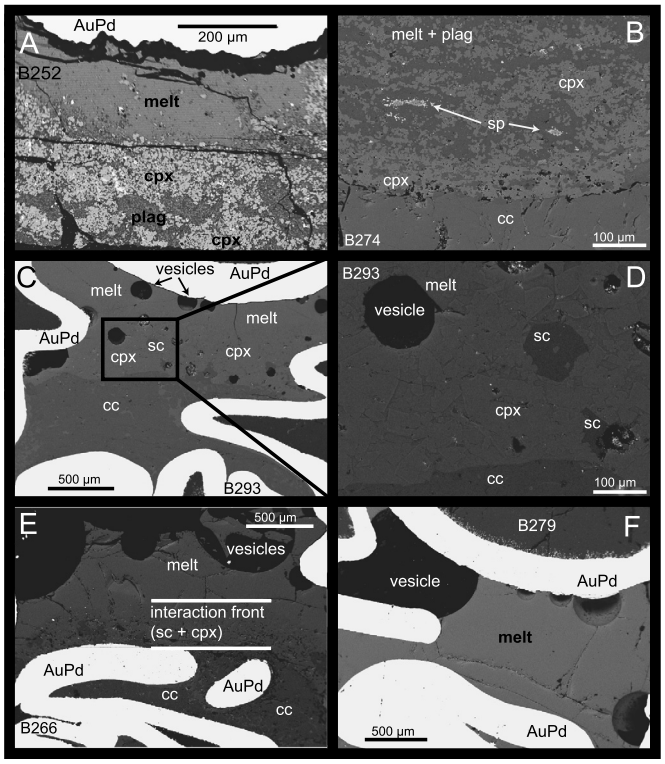

Fig. 1. Back-scattered electron (BSE) images displaying various textures of our experimental run products, arranged by increasing assimilation. (A) Run B252 (1.0 GPa, 1100 °C) shows a calcite-free assemblage of melt, plagioclase, and clinopyroxene (orthopyroxene and spinel not shown). (B) A high magnification image of the interaction front of experiment B274 (0.8 GPa, 1100 °C) exemplifies low-temperature phases of calcite (cc), clinopyroxene (cpx), spinel (sp), and small plagioclase (plag) grains within the melt. (C) Experiment B293 (1.0 GPa, 1175 °C) also contains scapolite (sc) in the interaction front. (D) A close-up of the vertical layering in B293 shows euhedral scapolite and clinopyroxene adjacent to residual calcite. (E) Experiment B266 (0.8 GPa, 1200 °C) shows the typical low-temperature capsule texture: a calcite base, clinopyroxene-rich interaction front in the middle, and melt (±vesicles) at the top. (F) Run no. B279 (0.5 GPa, 1200 °C) shows the high-temperature coexistence of glass and large vesicles and no other silicate mineral phases (residual calcite present at the bottom of the capsule, not shown).

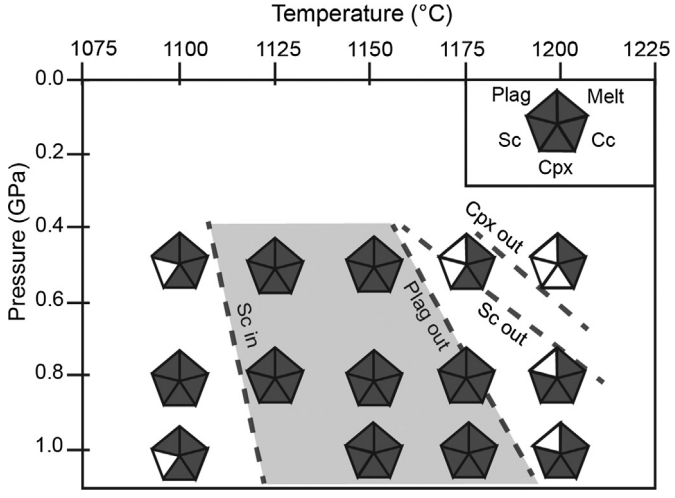

Fig. 2. A pressure–temperature plot showing major phases present in each experiment, where filled triangles indicate presence, and open triangles indicate absence of a phase. Major phases include Cpx = clinopyroxene, Plag = plagioclase, Sc = scapolite, Cc = calcite, and Melt. Exhaustion and appearances of major phases are denoted by dashed, labeled lines.

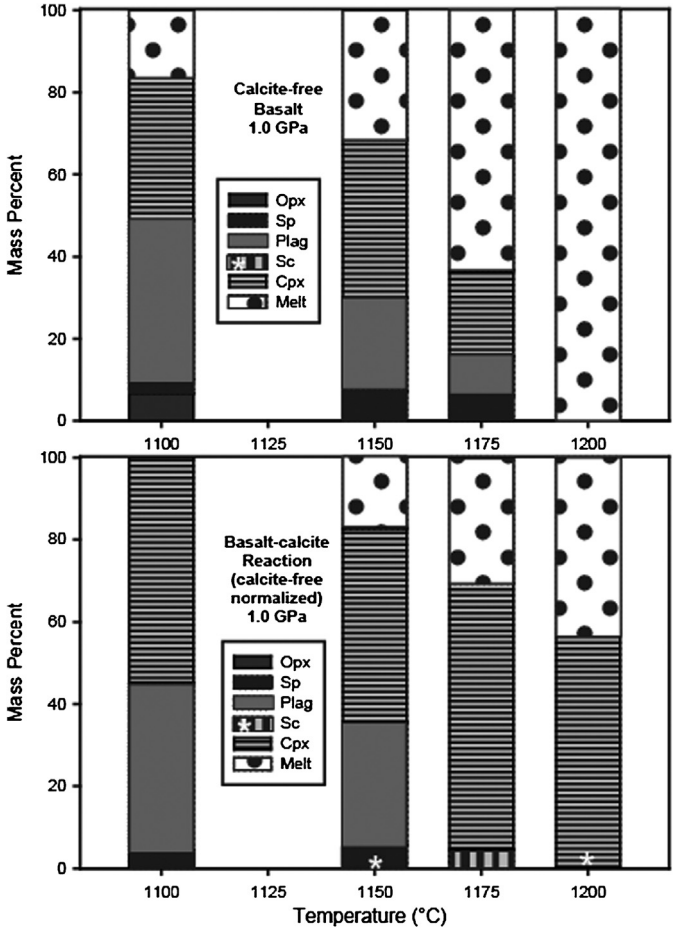

Fig. 3. A bar chart depicting the modal proportions of phases (in weight percent) present at 1.0 GPa crystallization interval of our model hydrous basalt (top) and in hydrous basalt–calcite reaction experiments (bottom) as a function of temperature (°C). Modal proportions are calculated on a volatile-free basis as reported in Table 1. Asterisk represents the presence of scapolite as a trace phase (near 0.0 in modal proportion).

(<5 wt.%; Table 1) of spinel-magnetite solid-solution are present at low temperatures at 1.0 GPa and all temperatures at 0.8 and 0.5 GPa.

Calcite-absent experiments depict a homogeneous texture of melt ± subhedral to euhedral grains of clinopyroxene, plagioclase, and spinel (1.0 GPa, >1175 °C; Fig. 1; ± orthopyroxene at 1100 °C only). This constrains the 1.0 GPa liquidus temperature (T_L) for the basaltic starting material at 1175–1200 °C. Interaction with calcite elevates the T_L of the silicate subsystem to >1200 °C at the same pressure. Normalizing phase proportions in 1.0 GPa basalt–calcite experiments to calcite-free percentages permits direct comparison with the silicate assemblage of subliquidus basalt (Fig. 3). Besides the elevation of T_L and lowered melt proportions at identical temperatures, a direct impact of interaction with calcite is an increase in clinopyroxene abundance along the liquid line of descent of our hydrous basalt, placing it in the majority over all other silicate phases (~56–65 wt.%, 1100–1200 °C, 1.0 GPa). Plagioclase, on the other hand, does not change perceptibly in abundance, but is exhausted at a lower temperature when calcite is present and scapolite appears; plagioclase is exhausted between 1175 and 1200 °C in calcite-free experiments, and between 1150 and 1175 °C in calcite-bearing experiments at 1.0 GPa (Table 1, Fig. 3). At 1.0 GPa, calcite-reacted assemblages also contain carbonate-scapolite (4.5 wt.% at 1150 °C only), which is absent in CO_2-free experiments. On the other hand, basalt crystallizes orthopyroxene at 1100 °C, a mineral not stable in experiments with calcite.

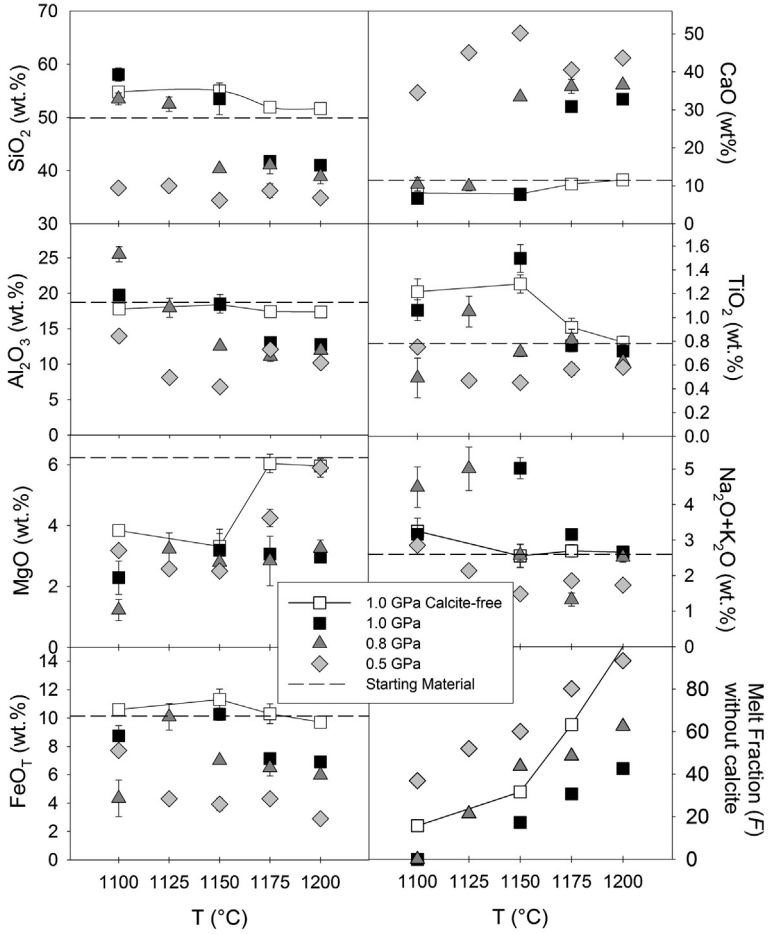

Fig. 4. Plots depicting the major element oxide geochemistry of experimental glasses (in wt.%, on a volatile-free basis, as reported in Table 2) as a function of temperature (in °C). The solid line with white squares represents calcite-free experiments, while closed symbols are the result of basalt–limestone interactions at 1.0 GPa (black squares), 0.8 GPa (dark gray triangles), and 0.5 GPa (light gray diamonds). The black dashed lines represent the starting composition on a volatile-free basis (see Table 2).

3.2. Phase chemistry

The major element chemistry of experimental glasses, on a volatile-free basis, and residual minerals clinopyroxene, plagioclase, and scapolite as determined using an electron microprobe are provided in Table 2 and Supplementary Tables 2–4, respectively.

3.2.1. Melt

Compositional evolution of silicate glasses on a volatile-free basis is shown in Fig. 4 as a function of temperature and plotted in a total alkali versus silica classification diagram in Fig. 5. At 1.0 GPa, the liquid line of descent of hydrous basaltic melt alone follows more subtle geochemical variation than calcite-contaminated glasses at the same pressure (Fig. 5). For the most part, without assimilation, silica and alumina contents are both fairly constant (53.2 ± 1.6 wt.% SiO_2, 17.8 ± 0.6 wt.% Al_2O_3) at all T, evolving from basaltic-andesite to basalt at higher temperatures (Fig. 5). CaO, too, shows little variation without a calcite buffer, increasing from 8.1 to 11.7 wt.% between 1100 and 1200 °C (Table 2). These melts are overall more magnesium- and iron-rich than their calcite-reacted counterparts. FeO_T shows minor variation, whereas MgO has an overall positive correlation with temperature. The alkalis behave as expected for incompatible elements, with initial enrichment at low melt fraction followed by steady dilution as F increases (Table 2, Fig. 4).

In comparison, melts from calcite-bearing experiments at 1.0 GPa geochemically differ most notably and expectedly in their CaO contents (Fig. 4). Increasing with temperature, CaO nears

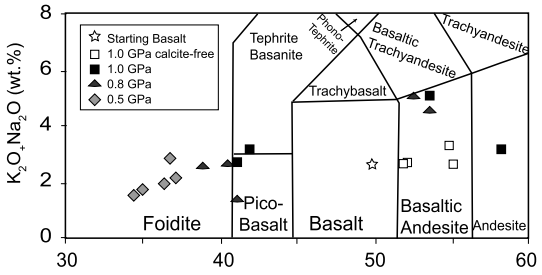

Fig. 5. Experimental glasses plotted on a TAS (Total Alkali versus Silica) diagram. Melts contaminated by limestone assimilation are filled symbols (black squares at 1.0 GPa, dark gray triangles at 0.8 GPa, and light gray diamonds at 0.5 GPa), while calcite-free basalt-only experiments are open symbols and the open star represents the starting basalt composition. Low T–high P reacted melts are largely andesitic and basaltic-andesitic, whereas high T–low P melts are foiditic.

calcite-free levels at low temperatures (<7 wt.% at ≤1150°C, 1.0 GPa), but reaches up to 32.8 wt.% at 1200 °C and same pressure. Calcium is inversely correlated to silica, such that substantial calcite assimilation (e.g., $T \geq 1175$ °C) exacerbates the diminishing silica content with increasing temperature (at 1200 °C, 1.0 GPa minimum SiO_2 = 41.0 wt.%; Table 2) and, to a lesser extent, aluminum content in the melt. The trend of increasing MgO with increasing temperature is observed but dampened ($<\pm1$ wt.% MgO variation, all T; Table 2) by limited extent of melt production caused by interaction with calcite. FeO_T of calcite-reacted basalt follows a similar trend to that of the calcite-free basalt with rising temperature, though lower in value (Fig. 4).

Table 2
Major element composition of starting melt and experimental glasses (in wt.%).

Run no.	Basalt[a]	B252*	B291*	B294*	B262*	B292	B306	B293	B263	B274	B297	B264	B283	B266	B267	B295	B298	B280	B279
n		21	13	16	20	17	10	20	7	6	6	9	9	31	7	7	8	51	49
SiO_2	49.89	54.8(3)	55.0(5)	51.9(5)	51(1)	58(1)	54(3)	41.7(4)	41.0(7)	53(1)	52(1)	40.3(5)	41(2)	39(1)	36.7(5)	37.1(7)	34.4(1)	36(1)	34.9(7)
TiO_2	0.78	1.2(1)	1.28(8)	0.92(8)	0.82(6)	1.06(9)	1.5(1)	0.76(5)	0.72(5)	0.5(2)	1.1(1)	0.71(4)	0.81(9)	0.63(4)	0.75(3)	0.47(2)	0.45(2)	0.56(5)	0.58(4)
Al_2O_3	18.71	17.8(1)	18.4(6)	17.4(5)	17.5(4)	19.7(7)	19(1)	13.1(2)	12.8(2)	25(1)	18(1)	12.5(2)	11.1(7)	12.0(5)	14.0(3)	8.1(2)	6.8(5)	12.1(5)	10.2(2)
FeO_T	10.14	10.6(3)	11.3(7)	10.3(7)	10.0(2)	8.7(7)	10.3(4)	7.14(1)	6.9(2)	4(1)	10.1(9)	7.0(1)	6.5(6)	6.0(2)	7.7(1)	4.3(2)	3.9(4)	4.31(9)	2.90(7)
MnO	0.21	0.25(2)	0.27(4)	0.25(3)	0.26(3)	0.24(4)	0.29(4)	0.25(3)	0.22(3)	0.14(3)	0.32(5)	0.25(3)	0.22(4)	0.22(4)	0.29(4)	0.17(4)	0.14(3)	0.17(3)	0.16(4)
MgO	6.24	3.8(1)	3.3(4)	6.0(3)	6.2(2)	2.3(5)	3.2(7)	3.07(8)	2.96(5)	1.2(4)	3.2(5)	2.80(7)	2.8(8)	3.3(3)	3.18(8)	2.58(5)	2.5(2)	4.3(3)	5.9(3)
CaO	11.43	8.1(2)	7.8(2)	10.4(2)	11.7(1)	6.7(6)	7.7(7)	30.8(2)	32.8(2)	10(2)	10(1)	33.4(4)	36(2)	36.5(9)	34.5(3)	45.0(5)	50.2(7)	41(1)	43.7(7)
Na_2O	2.08	2.5(1)	1.6(3)	2.1(2)	2.25(6)	1.7(3)	3.2(2)	2.5(1)	2.05(4)	3.5(4)	3.6(6)	2.3(1)	1.1(2)	2.0(2)	2.45(6)	1.9(1)	1.33(7)	1.5(1)	1.40(8)
K_2O	0.52	1.00(3)	1.0(1)	0.58(5)	0.49(4)	1.4(1)	1.9(2)	0.64(4)	0.57(2)	1.0(4)	1.4(3)	0.66(2)	0.21(4)	0.53(3)	0.40(2)	0.24(3)	0.15(3)	0.35(2)	0.33(2)
Sum[b]	100.00	100.0(6)	100.0(6)	100.0(7)	100(2)	100.0(7)	100(3)	100.0(4)	100.0(9)	100.0(8)	100.0(9)	100.0(8)	100(2)	100(2)	100.0(8)	100(1)	100(1)	100(2)	100(1)
Est. $H_2O + CO_2$[c]	4.03	3.1	6.3	3.0	5.1	6.8	7.0	12.3	10.6	–	3.4	13.1	11.5	10.7	13.5	10.1	13.4	17.8	19.6
CaO/Al_2O_3[d]	0.6	0.5	0.5	0.7	0.8	0.4	0.5	2.7	2.6	0.5	0.6	2.7	3.3	3.1	2.5	5.6	8.6	3.4	4.3

* Experiments with starting hydrous basalt composition only; all others performed with 50 wt.% basalt and 50 wt.% calcite.

[a] Basalt is the starting composition reported on a volatile-free basis based on weighed proportion of reagents (see Supplementary Table 1); slight compositional deviation from superliquidus run B262* likely chiefly due to minor iron loss to the AuPd capsule.

Number in (parentheses) is one sigma standard deviation for *n* is the number of EMPA spot analyses averaged for obtaining composition of each phase reported in least digits cited, i.e., 54.8(3) should be read as 54.8 ± 0.3 wt.%. FeO_T is total iron content ($FeO + Fe_2O_3$).

[b] Sum indicates total recalculated on volatile-free basis.

[c] Est. $H_2O + CO_2$ is volatile content based on deficit of analytical sum from 100 wt.%; errors are identical to those given for Sum for each experiment. H_2O is the only volatile in the case of the starting basalt composition.

[d] CaO/Al_2O_3 weight ratio refers to the section on ultracalcic melts.

In run no. B283 two silicate melts were identified; where a negligible proportion of unreacted silicate melt exists only in the far reaches of the uppermost corners of the capsule, likely impeded from mixing due the build-up of a thick cpx interaction front, the 'reacted melt' near the interface is instead presented in the table.

In limestone–basalt reactions, the extent of assimilation increases with decreasing pressures and the extent of melt contamination extends to lower temperatures at lower pressures. For example, whereas at 1.0 GPa melts become about a third CaO by weight at ≥1175 °C, glasses at 0.8 GPa reach this level at a temperature of ≥1150 °C, after which they maintain a subtle increase with temperature. This trend is seen in all 0.5 GPa experimental melts (Fig. 4), with slight deviation above 1150 °C as a function of dilution by increasing F. In contrast, with lowering pressure, silica decreases with similar magnitude to CaO. Partial melts at 1.0 GPa are andesite to basaltic-andesite (>53 wt.% SiO_2; Fig. 5) at <1175 °C, while glasses formed at 1175 and 1200 °C fall on the border of foidite and pico-basalt (~41–42 wt.% SiO_2; Fig. 5). At 0.8 GPa, basaltic-andesite is only generated at 1100 °C, whereas melts formed at ≥1150 °C are foidites (Fig. 5). Lowering the pressure to 0.5 GPa again lowers the temperature at which the silica content is foiditic (~34–37 wt.% SiO_2, all T; Fig. 5). Alumina decreases with increasing temperature in all calcite-bearing experiments, with lower pressures and higher temperatures (Fig. 4). The opposite is true of MgO, which increases with decreasing pressure and increasing temperature. Similar to 1.0 GPa, in the presence of calcite, FeO_T in 0.8 GPa melts first increases below 1150 °C and then decreases (10.1–5.9 wt.% FeO_T at 1125 °C to 1200 °C; Table 2, Fig. 4).

3.2.2. Clinopyroxene

Clinopyroxene is present in nearly all experiments (Table 1). The distinction between calcite-free and calcite-bearing experiments across all T at 1.0 GPa is defined by more magnesian (Mg# ~52.4–74.7 calcite-free; 51.7–64.8 calcite-bearing) and silicic (SiO_2 ~48.4 ± 0.9 wt.% calcite-free; ~45.1 ± 4.2 wt.% calcite-bearing) clinopyroxene in the first, and more aluminous (Al_2O_3 ~7.3 ± 0.6 wt.% calcite-free; ~12.9 ± 5.5 wt.% calcite-bearing) and calcic (CaO ~18.0 ± 1.0 wt.% calcite-free; 20.8 ± 3.3 wt.% calcite-bearing) clinopyroxene in the second (Supplementary Table 2). The range of enstatite and ferrosilite components of clinopyroxene formed during assimilation at 1.0 GPa, for example, are significantly lower at T >1150 °C (En + $Fs_{35.4–37.3}$) as compared to calcite-free clinopyroxene at the same pressure (En + $Fs_{66.0}$), in contrast to the wollastonite component ($Wo_{24.1}$ calcite-free, $Wo_{36.7–38.2}$ calcite-bearing; Supplementary Table 2, Fig. 6) based on an En + Fs + Wo + CaTs normalization.

Within basalt–calcite experiments, increasing temperature and decreasing pressure causes clinopyroxene to become more calcic and aluminous (19.3 to 25.8 wt.% CaO and 8.7 to 20.6 wt.% Al_2O_3, from 1100 °C, 1.0 GPa to 1175 °C, 0.5 GPa; Supplementary Table 2). Aluminum and silica display opposing trends with temperature (Fig. 6) whereby silica ultimately reaches anomalously low values for a typical clinopyroxene (e.g., 8.3 to 17.9 wt.% Al_2O_3, 45.7 to 41.0 wt.% SiO_2, from 1100 to 1200 °C, 0.8 GPa). Therefore, with increasing interaction between the basalt and calcite, clinopyroxene becomes Ca-Tschermak-rich (e.g., $CaTs_{40.7}$ at 0.5 GPa, 1175 °C; Supplementary Table 2, Fig. 6).

3.2.3. Plagioclase

All plagioclase compositions in this study are anorthite-rich ($An_{47.0–60.3}$ $Ab_{35.9–48.9}Or_{1.2–6.9}$). Plagioclase in calcite-free experiments ($An_{48.7–53.3}$, 1100 to 1175 °C, 1.0 GPa) differs little from plagioclase formed in the presence of calcite ($An_{48.1–49.1}$, 1100–1150 °C, 1.0 GPa; Supplementary Table 3). With decreasing pressure, calcite-saturated plagioclase becomes more anorthitic (e.g., $An_{57.1–60.3}$ at 0.5 GPa, 1100–1125 °C). Temperature effects on plagioclase composition are less evident due to the limited T-stability of plagioclase.

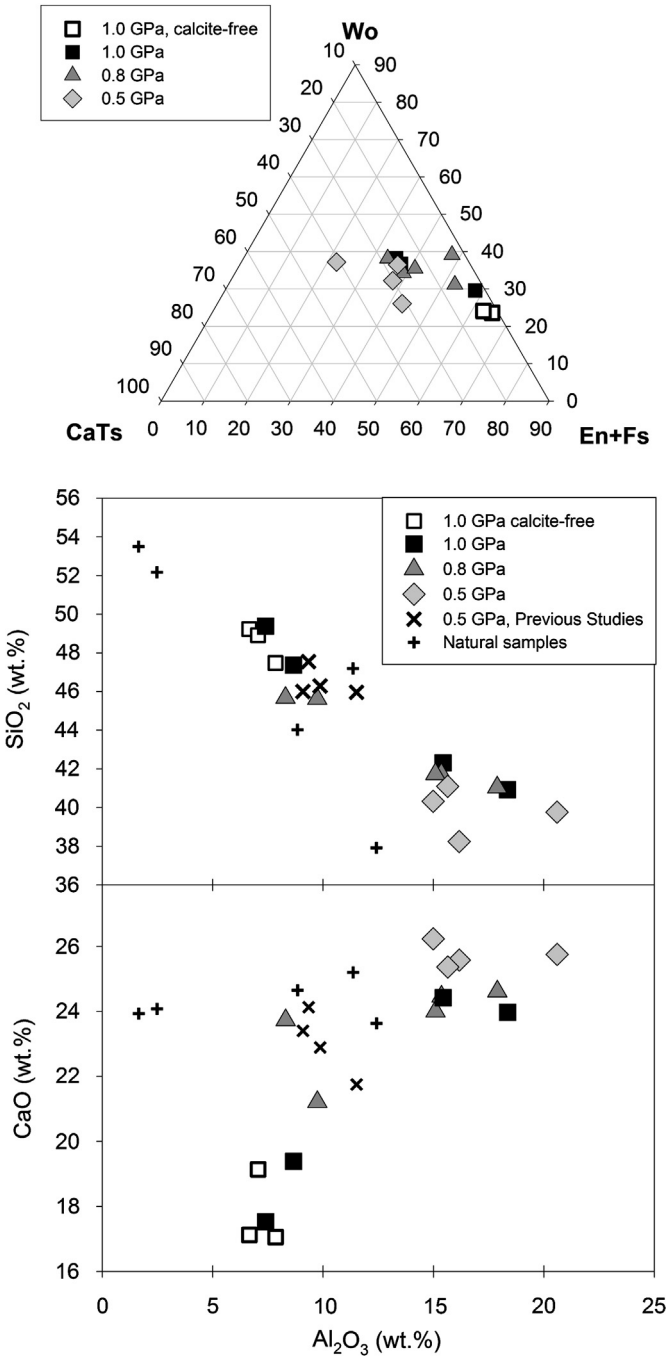

Fig. 6. Ternary diagram shows the clinopyroxene trend toward a Ca-Tschermak (CaTs; $CaAlAlSiO_6$) end-member with increasing T and decreasing P at the expense of Enstatite + Ferrosillite (En + Fs; $(Mg,Fe)_2Si_2O_6$) with similar Wollastonite components (Wo; $CaSiO_3$). The graphs of oxide concentrations confirm these elemental changes with respect to temperature (increasing to the right) and pressure for this study (symbols as in Fig. 5) and previous studies at 0.5 GPa (×, Freda et al., 2008; Iacono-Marziano et al., 2007; Mollo et al., 2010), and natural clinopyroxene in carbonate-assimilating systems (+, Freda et al., 2006; Gaeta et al., 2009; Goff et al., 2001).

3.2.4. Scapolite

The general formula of scapolite can vary, depending on the volatile available $[(Ca,Na,K)_4(Al,Si)_{12}O_{24}(CO_3,SO_2,OH,Cl,F)]$. However, with high X_{CO_2} and no source of chlorine, fluorine or sulfur, this study produces the calcic end-member, Meionite ($Ca_4Al_6Si_6O_{24}CO_3$) (Supplementary Fig. 1). Using a 12-anion normalization we determine nearly consistent atomic proportions of silica and aluminum across various P–T conditions ($Si_{6.2–6.6}Al_{5.8–5.4}$),

and a strong calcium dominance over sodium ($Ca_{3.6-4.3}Na_{0.5-0.01}$). Meionite percentage calculations [% Me; determined by Ca/(Ca + Na + K) × 100] of (Evans et al., 1969), which conform well to the earlier cation-based Meionite calculation of (Shaw, 1960; see Supplementary Fig. 1 inset), demonstrate exceedingly little solid solution in our scapolites ($Me_{94.1-98.1}Ma_{5.9-1.9}CO_3$; Supplementary Table 4). Variation in % Me indicates only a slight increase with decreasing pressure and increasing temperature. Another method of scapolite quantification is the Equivalent Anorthite content [Eq An; (Al-3)/3 × 100; Moecher and Essene (1990)], which is less directly proportional to percent-assimilation of our experiments, but is similarly quite high (Eq An = 80.5–94.5; Supplementary Table 4).

4. Discussion

4.1. Experimental phase relations of limestone assimilation by hydrous arc basalts

Our experiments allow us to constrain the nature of shift of basalt crystallization owing to interaction with calcite along its liquid line of descent at a single pressure and also above the basalt liquidus as a function of pressure. At low temperatures (e.g., 1.0 GPa, 1100 °C), basalt and limestone interaction is responsible for the production of clinopyroxene, plagioclase, and CO_2 according to the following:

$$4CaCO_3\ (\text{calcite}) + Al_2O_3\ (\text{melt}) + 4SiO_2\ (\text{melt}) = CaAl_2Si_2O_8\ (\text{plag}) + Ca_2Si_2O_6\ (\text{cpx}) + CaO\ (\text{melt}) + 4CO_2\ (\text{fluid}) \quad (2)$$

Taking into account crystallization of basalt and change in modal proportions, adding calcite alters the phase assemblage at 1.0 GPa, 1100 °C, on a volatile-free basis, according to the following reaction:

$$0.43\text{opx} + 0.21\text{cc} + 1.00\text{melt} \rightarrow 0.08\text{sp} + 0.22\text{plag} + 1.34\text{cpx} \quad (3)$$

where opx = orthopyroxene, cc = calcite, sp = spinel, plag = plagioclase and cpx = clinopyroxene, which indicates that interaction with calcite shifts the mineralogy along the liquid line of descent from orthopyroxene to clinopyroxene and also produces plagioclase and minor spinel as the melt fraction is diminished. Although the above reaction is expressed on a volatile-free basis, consumption of calcite suggests that reactive crystallization of each gram of initial basaltic melt leads to the release of 0.09 g of CO_2 in the fluid plus reacted melt.

At an intermediate temperature (e.g., 1.0 GPa, 1175 °C), plagioclase and spinel are instead consumed, with production of clinopyroxene and scapolite, such as:

$$0.23\text{sp} + 0.35\text{plag} + 0.64\text{cc} + 1.00\text{melt} \rightarrow 0.19\text{sc} + 2.03\text{cpx} \quad (4)$$

where sc = scapolite. Equation (4) generates three times as much CO_2 (0.28 g) per 1.00 g of reacting melt as reaction (3), of which only 0.015 g (5%) is locked in scapolite. At high temperature, (1200 °C, 1.0 GPa), the initial basaltic melt is above its liquidus, whereas in the presence of calcite, clinopyroxene is present. As such, melt and calcite are consumed, while cpx (and trace scapolite) is produced:

$$0.41\text{cc} + 1.00\text{melt} \rightarrow 1.41\text{cpx} \quad (5)$$

At low pressure, high temperature (e.g., 0.5 GPa, 1200 °C), also above the liquidus of our starting basalt, all silicate phases that were crystallized at lower temperatures—scapolite, plagioclase, and clinopyroxene—have entered the contaminated melt:

$$1.26\text{cc} \rightarrow 1.00\text{melt} + 0.26\text{sp} \quad (6)$$

Overall, the range of reactions produced in this study can be summarized as follows:

$$\text{Cc} + \text{basalt/basaltic-andesite melt} + \text{cpx} \pm \text{plag} \rightarrow \text{foiditic melt} + \text{sp} \pm \text{cpx} \pm \text{plag} \pm \text{sc} + \text{C–O–H fluid} \quad (7)$$

Though different in proportion, the near-identical calcium content in plagioclase regardless of calcite involvement suggests carbonate breakdown has little effect greater than the basalt composition on the chemistry of this mineral. However, with increasing temperature, calcium is reincorporated into scapolite. The combined consumption of feldspar and calcite results in high CaTs proportion in clinopyroxene, best expressed by the following reaction:

$$CaAl_2Si_2O_8\ (\text{plag}) + CaMgSi_2O_6\ (\text{cpx}) + 4CaCO_3\ (\text{cc}) + 3Al_2O_3\ (\text{melt}) + 3SiO_2\ (\text{melt}) = CaAlAlSiO_6\ (\text{cpx}) + Ca_4Al_6Si_6O_{24}CO_3\ (\text{sc}) + MgO\ (\text{melt}) + CaO\ (\text{melt}) + 4CO_2\ (\text{fl}) \quad (8)$$

Assimilation of up to 47.6 wt.% calcite produces slightly less than half that amount (44 wt.%, by stoichiometry) of CO_2, which is incorporated primarily into the vapor phase but also to some extent into scapolite as well as melt (up to ~20 wt.% C–O–H volatiles, by chemical analysis deficit, though there may be minor Na-loss that may decrease the volatile content by a few wt.%; Table 2). It has been reputed that the presence of scapolite with calcite constrains the X_{CO_2}, but further work is needed to extrapolate both the low temperature experiments of (e.g., Aitken, 1983), and the "An + Cc → Sc" join on the phase diagram of Moecher and Essene (1990) to our ≥1100 °C and multicomponent system in order to obtain realistic X_{CO_2} values.

4.2. Phase equilibria of carbonate–basalt interaction—comparison with previous experimental studies

Although this study uniquely contains scapolite, the phlogopite and olivine produced in CAVD experiments (Conte et al., 2009; Freda et al., 2008; Iacono-Marziano et al., 2007; Mollo et al., 2010) are distinctly lacking in this study. The missing mica is likely due to our low level of hydration (Conte et al., 2009). Modal increase in clinopyroxene can reduce the stability of olivine (Barnes et al., 2005), but calcite-free experiments were similarly olivine-absent (Table 1), implying the control of starting melt composition is also likely key.

Elevating Al_2O_3/SiO_2 ratios in clinopyroxene with increasing temperature and increasing carbonate consumption (Fig. 6) mirrors those from several previous studies. A low-temperature, high-pressure decrease in the mafic components within clinopyroxene may explain the initial increase in total iron concentration in coexisting melts between low and intermediate temperature at 0.8 and 1.0 GPa (Figs. 4, 6). As in the experiments of Mollo et al. (2010), clinopyroxene is the final liquidus phase, stable to higher temperatures in the presence of excess calcite (>1200 °C, 1.0 GPa) than calcite-free runs (<1200°C, 1.0 GPa), defining an elevated liquidus with the addition of carbonate (e.g., Freda et al., 2008; Gaeta et al., 2009).

4.3. Comparing experimental residual assemblage with natural occurrences of magma–carbonate and fluid–carbonate reaction products

The phases that make up our low-temperature basalt–limestone products—plagioclase, clinopyroxene, spinel—are very similar to those found in natural carbonate-assimilating lavas at Merapi, Norway, and Popocatepetl (Barnes et al., 2005; Chadwick et al., 2007; Di Rocco et al., 2012; Goff et al., 2001; Troll et al., 2012) as well as—anorthite and CaTs end-members in particular—in exoskarns (e.g., Gaeta et al., 2006; Kerrick, 1977). In affirmation of CAVD experiments, olivine and phlogopite were identified in natural Italian rocks (Di Rocco et al., 2012), in contrast to our assemblage. Yet the unique presence of scapolite in our experiments aligns with a common occurrence in exoskarns (Aitken, 1983; Iacono-Marziano et al., 2008), including the Somma–Vesuvius complex in Italy (e.g., Kuhn, 2005). Scapolite is an excellent indicator of volatile-rich fluids in metamorphic rocks, including marbles, skarns, syenite, calcareous gneiss, granulite around the world (e.g., Moecher et al., 1994; Shaw, 1960), though only previously found as a result of primary igneous processes in diatremes (Aitken, 1983). The igneous assemblage in our experiments deviates from a typical metamorphic coexistence with quartz, wollastonite, zoisite, garnet, ± sphene, ± mica, ± amphibole (Barnes et al., 2005; Di Rocco et al., 2012; Einaudi and Burt, 1982; Freda et al., 1997; Gaeta et al., 2006; Kerrick, 1977), hence having scapolite in equilibrium with clinopyroxene and occasional anorthite as in our 1125–1175 °C experiments at 0.8 GPa, classifies the reaction front as an igneous endoskarn (Moecher and Essene, 1990). The absence of garnet results in enriching our clinopyroxene in CaTs. This study synthesized an extreme calcic composition of scapolite that nature rarely realizes; intermediate (e.g., Mizzonite) compositions tend to be more stable, because Al–O and Si–O bond disorder increases with temperature and aluminum—and thus Eq An and Meionite—content (Moecher and Essene, 1990). It is likely due to this bonding issue that our scapolites, being more Meionitic than natural samples, do not align linearly with Equivalent Anorthite content (Supplementary Fig. 1).

4.4. Contaminated melts

4.4.1. Major element composition variation

Melts assimilating more than a few weight percent calcite are silica-undersaturated, possessing 34.4–41.8 wt.% SiO_2, as much as 30.8–50.2 wt.% CaO, and $\leq\sim$10–20 wt.% CO_2–H_2O volatiles (Table 2). The correlation between increasing calcium and silica-depletion is unsurprising given that CaO dilutes the SiO_2 content of the melt. We note that the major element variations between decreasing pressures have similar if not more significant trends as compared to those caused by increasing temperature (Fig. 4), a factor that has been largely disregarded in previous work (e.g., Deegan et al., 2010). The depth at which the assimilation is occurring can impact assimilant proportion and the resulting products.

Without the enhanced K_2O, which is typical of Italian lavas, our contaminated glasses belong to a low-alkali foiditic classification as opposed to experimental and natural trachytes, K-trachybasalts, phonotephrites, tephriphonolites and K-foidites, which contain up to 50 wt.% silica (Freda et al., 2008; Gaeta et al., 2006; Iacono-Marziano et al., 2008, 2007; Mollo et al., 2010).

4.4.2. Ultracalcic melts

Our calcite-assimilated melts also potentially have implications for natural ultracalcic melts (identified globally in mid-ocean ridge, oceanic island, back-arc, and also in arc settings such as the Philippines, Indonesia, Sunda Arc, Papua New Guinea, Central America, Antilles, and Italy; Schiano et al., 2000 and references therein). Ultracalcic melts are loosely defined by their calcium content (CaO $\geq$13.5 wt.%; up to 19 wt.% naturally, Medard et al., 2004), calcium-to-aluminum ratio (CaO/Al_2O_3 >1.0; up to $\sim$1.50 naturally, Marchev et al., 2009; Sigurdsson et al., 2000) and tend to be highly alkalic (>2 wt.% $Na_2O + K_2O$) particularly at volcanic arcs. Ultracalcic samples are broken down into two groups: hypersthene- and nepheline-normative. The latter, being SiO_2-poor (44–47 wt.% SiO_2), alkali-rich ($\geq$3 wt.%) and typically associated with arc settings (Kogiso and Hirschmann, 2001; Medard et al., 2004), aligns best with carbonate-assimilated glasses. Existing studies favor the idea that extreme enrichment in CaO is derived from either pure or mixed (e.g., 40:50 pyroxenite–peridotite ratio, Sorbadere et al., 2013) lower-crustal pyroxenite (e.g., 'Experimental lherzolite melts,' Fig. 7, references in the Supplementary materials). As a caveat, the pyroxenite would have to contain amphibole in order to provide sufficient water to lower melting temperature to subarc crustal conditions (e.g., >1190 °C, 1.0 GPa, Medard, 2006).

The glasses from our own carbonate-assimilation study as well as those of Iacono-Marziano et al. (2008) and Conte et al. (2009) represent some of the most ultracalcic melt compositions generated experimentally at mid-crustal pressures (Fig. 7 and inset). Ultracalcic criteria were achieved at >1175 °C at 1.0 GPa, >1150 °C at 0.8 GPa, and all T at 0.5 GPa in this study, with a similar clinopyroxene and spinel-rich residue to the ultracalcic finds of Green et al. (2004), Medard (2006), and Conte et al. (2009). In contrast, lherzolite experiments (Fig. 7; references in the Supplementary materials) produce melts with CaO contents too low at a given CaO/Al_2O_3, deviating from the linearity of the CaO and CaO/Al_2O_3 relationship. At high CaO/Al_2O_3 values, amphibole-bearing wehrlite partial melts (Medard, 2006) also display low CaO contents, and experiments require high melt fractions ($F > 0.3$, 1.0 GPa; $F > 0.4$, 0.5 GPa) to reach ultracalcic melt compositions.

Ultracalcic melt inclusions are found typically in olivine or spinel phenocrysts within arc lavas (e.g., Kogiso and Hirschmann, 2001) and if the signature is extensive enough, the bulk rock may be ankaramitic (e.g., Vanuatu arc, Schmidt et al., 2004). In fact, some of these ultracalcic melt inclusions have been discovered in Italy where carbonate assimilation is abundant (Conte et al., 2009). The natural samples, taken from arcs all over the world (see references in Fig. 7), hover right around the ultracalcic distinction mark, often exceeding only one (CaO or CaO/Al_2O_3) ultracalcic minima, whereas melts with ingested carbonate easily bypass both qualifications at higher melt fractions (F >0.15). Mixing our melts with uncontaminated primary basaltic melt in e.g., a 1 to 3 ratio at 1.0 GPa (see mixing lines in Fig. 7), or basalt interaction with impure limestone could lower the CaO contents of experimental ultracalcic melts to those of natural ultracalcic samples. Nonetheless, there lies a true similarity in mineral assemblage (e.g., CaTs clinopyroxene ± feldspar ± spinel, Medard, 2006) and melt composition. We therefore propose that ultracalcic melts in many arc settings may be the result of intrusions of basalt into carbonated sediments in the upper plate, preserved in the stages of early interaction and/or generation of clinopyroxenites, which could be potential source lithology of ultracalcic melts, may occur through limestone–basalt interaction at arc crust.

4.5. The extent of limestone assimilation

The relative lack of chemical variability of all melts at 0.5 GPa and high-temperature melts at 0.8 and 1.0 GPa (Fig. 4) suggests that a maximum carbonate assimilation for our investigated basaltic composition is $\sim$48% at 1200 °C, 0.5 GPa. The limiting factor preventing further contamination in other equilibrium studies of similar conditions (e.g., Freda et al., 2008; Mollo et al., 2010) is thus the amount of carbonate added, permitting the melt's abundance to dampen the extent of assimilation. This extent of contam-

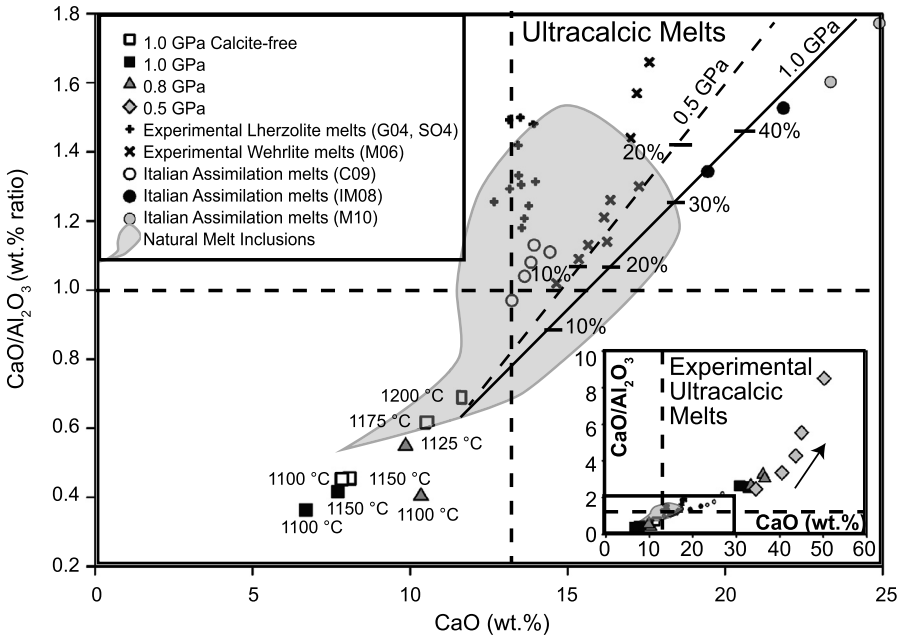

Fig. 7. CaO/Al_2O_3 wt.% ratio versus CaO content (wt.%) comparing experimental and natural melt compositions considered 'ultracalcic' (CaO/Al_2O_3 >1.0 and CaO content >13.5 wt.%; represented by dashed lines). Data for natural ultracalcic melt inclusions (gray region) are identified in the Supplementary materials. At high-*T*, low-*P*, CaO/Al_2O_3 of calcite contaminated melts produced in this study (symbols as in Fig. 5) far exceed (see inset, with black rectangle outlining the larger graph area) those of natural samples as well as those produced in previous carbonate assimilation (circles) and lhzerzolite ('+' symbols) and wehrlite ('x' symbols) melting experimental studies, all of which are referenced in the Supplementary materials. Temperatures for experiments are either labeled or indicated by an arrow as a trend of increasing temperature. Mixing between primary basalt (starting material composition, see Table 2) and calcite-assimilated melts are shown for 1.0 and 0.5 GPa at 1200 °C by solid and dashed lines, respectively; adding 10–30% of calcite-saturated magma can reach natural ultracalcic melt inclusion compositions.

ination exceeds estimates for natural systems (e.g., 14–15% assimilation at Vesuvius, Iacono-Marziano et al., 2009; 10% at Merapi, Chadwick et al., 2007; and 7% at CAVD, Gaeta et al., 2009); although it is thus likely that mixing with uncontaminated basalt that does not crosscut limestone, recharge, or depth of basalt–carbonate interaction could dampen carbonate contamination. Another possibility is the potential impurity of the crustal carbonates, i.e., additional assimilation of crustal silicates would likely diminish the carbonate signature.

Mollo et al. (2010) argued that decarbonation can be self-limiting without an outlet to release the CO_2 in the system. However, it is unlikely that a clinopyroxene-rich 'skarn barrier' is a restricting factor in further assimilation between the country rock and magma body (Gaeta et al., 2009) as our 1200 °C, 0.5 GPa experiment has no clinopyroxene layer separating the melt and calcite while consuming a negligible amount more calcite than the 25 °C cooler clinopyroxene-bearing experiment. Rather, the fact that the trend of increasing assimilation with decreasing *P* and increasing *T* tapers off when the melt possesses near-carbonatitic calcium contents (Table 2) suggests that the extent of assimilation can be self-limiting if and when assimilative capacity of the uncontaminated melt is reached. As the contaminated magma becomes CaO-rich, the mixed volatile solubility (based on EPMA difference) is ~20 wt.%. Although it could be that as melt CaO content increases, the solubility of CO_2 dissolved as CO_3^{2-} also increases (e.g., Dasgupta et al., 2013) given that CO_2 solubility is strongly affected by pressure, most of the volatiles dissolved in the glasses is likely to be H_2O.

In addition to the maximum extent of assimilation, the overall carbonate signature in the magmatic system may also be diluted by magma recharge or mixing. The melts produced in this study may additionally evolve during ascent and/or may be left behind as pyroxene-rich cumulates during crystallization. In fact, based on the major element composition, typical erupted arc basalts (excluding those with a significant 'carbonate' signature such as Vesuvius; PetDB: www.earthchem.org/petdb, Lehnert et al., 2000) can allow no more than 1.5 wt.% carbonate assimilation into primary arc basalt.

4.6. CO_2 emission at volcanic arcs

Following the method of Iacono-Marziano et al. (2007, 2009), we used a simple equation to extrapolate the total concentration of CO_2 dissolved in our experimental melts + fluids to volcano-scale estimates over a range of magmatic recharge rates typical for arc volcanoes (10^{10}–10^{14} g/y, Crisp, 1984; White et al., 2006; Fig. 8). We make the assumption that all digested carbon, as calculated by mass balance, some of which is dissolved in the melt at experimental pressures, ultimately exsolves and is released at the volcanic vent. For example, for a system with an average magmatic intrusion rate similar to Vesuvius (5.4×10^{12} g/y, Rosi et al., 1987), assuming constant recharge rate and wall-rock interaction, we calculate CO_2 emission between 5.1×10^{11} and 1.2×10^{12} g/y (Fig. 8) based on assimilation percentages expected at shallow depth (0.5 GPa) at 1100 °C (21.6 wt.%) to 1200 °C (47.6 wt.%). The lower end of this range is similar to observed measurement at the vent of 1.1×10^{11} g/y CO_2 (Fig. 8; Caliro et al., 2005; Frondini et al., 2004), agreeing with <~20% assimilation estimates for Vesuvius (e.g., Iacono-Marziano et al., 2009). If, on the other hand, assimilation is occurring at high temperature under Vesuvius, we estimate the reaction along the magma–carbonate interface would need to be diluted by an unreacted basaltic melt (containing an average CO_2 content of 3000 ppm, Wallace, 2005) amounting to 39% of the magma flux. Similarly, using magma ascent rates at Merapi (3.2×10^{12} g/y, Siswowidjoyo et al., 1995) we estimate 12–26% of the magma undergoes assimilation at 0.5 GPa, 1100–1200 °C in order to dilute our maximum CO_2 estimate (5.7×10^{12} g/y) to match the measured output (8.8×10^{10} g/y CO_2, Toutain et al., 2009). For the highly active Popocatepetl (7.2×10^{14} g/y magma flux, Roberge et al., 2009) and Etna (6.8×10^{13} g/y magma flux,

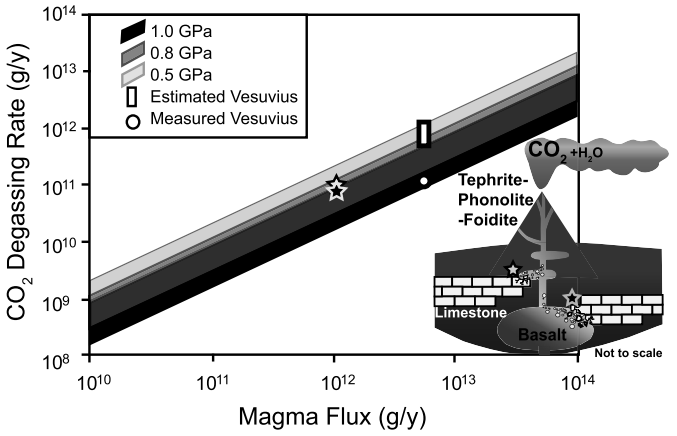

Fig. 8. Estimated CO_2 degassing rates from the upper plate over a range of magma recharge rates on a log–log scale, based on assimilation percentages produced at the *P–T* conditions of this study. Calculations assume a constant reaction rate, magma recharge rate, and a stoichiometric release of all 44 wt.% of consumed calcite as CO_2. The black shaded region is the range at 1.0 GPa between 1100 and 1200 °C; dark gray field is for 0.8 GPa, and light gray is at 0.5 GPa over the same *T* range. Given the Vesuvian magma supply rate (5.4×10^{12} g/y, Rosi et al., 1987), our maximum estimates of excess CO_2 at Vesuvius would be 5.1×10^{11} to 1.1×10^{12} (open rectangular bar), near to the measured Vesuvius value of 1.1×10^{11} g/y (open circle, Caliro et al., 2005; Frondini et al., 2004). Also shown for 10^{12} g/y magma flux rate are the expected equilibrium value of CO_2 degassing rates for a shallow, cooler (0.5 GPa, 1100 °C; light gray star, black rim) and a deeper, hotter (1.0 GPa, 1200 °C; black star, light grey rim) basalt–limestone interaction scenarios. Owing to the opposing effect of pressure and temperature on the extent of calcite assimilation by hydrous arc basalt, similar CO_2 degassing efficiency may be realized over a wide range of crustal-magmatic conditions. The inset shows a schematic summarizing the hydrous basalt–limestone interaction scenarios, with associated gray and black stars, in the continental arc crust as captured in this study.

Harris et al., 2011), at the same conditions, 6–13% and 41–92% of their magma would need to react with calcite to match their observed emission rates of 1.1×10^{13} g/y and 6.0×10^{12} g/y CO_2, respectively (Burton et al., 2013). Without factoring in the dilution effects of uncontaminated magma volume or impure carbonate, we suggest carbonate assimilation at these 4 volcanoes together can contribute at maximum an additional ≤ 1.25–17.2×10^{13} g/y CO_2 to the global arc flux, ignoring any carbon the intruding magma may already be carrying from the subduction-affected mantle wedge.

Based on the contamination calculated above for Vesuvius, Merapi, Etna and Popocatepetl, about 3% of global subaerial volcanic arc CO_2 emissions (2.71×10^{14} g/y total, Burton et al., 2013) may be crustally-derived, and based on a maximum global carbonate assimilation estimate (assuming all magma reacts with calcite) between 0.5 and 1.0 GPa at 1100–1200 °C this could extend to 4.6–63.4%. Global volcanic degassing estimates are generally oversimplified, relying on mantle carbon concentration, or on primitive basalt CO_2 content as a basis for the magmatic output (e.g., Dasgupta, 2013). Our study along with several previous studies (Di Rocco et al., 2012; Ganino and Arndt, 2009; Iacono-Marziano et al., 2009; Lee et al., 2013) underscore the importance of crustal carbon on exogenic–endogenic C-cycle connection at present and through time.

It has been speculated that during the late Cretaceous to early Paleogene the total extent of continental arcs interacting with crustal carbonates amassed to ~25% of the current total arc length (Lee et al., 2013). Presuming a vent spacing similar to that in the Cascades of every 100–150 km (Guffanti and Weaver, 1988), 87–130 volcanoes could experience carbonate assimilation at any given time. Interaction at ~15 km depth, with a magma intrusion rate averaged from Etna, Merapi, Vesuvius, and Popocatepetl, could degas up to 2.5–5.6×10^{15} g/y CO_2, or almost ≤ 5.6 Gt/y of crustal CO_2 to the atmosphere, which is 1–2 orders of magnitude greater than current total arc output estimates (Burton et al., 2013; Dasgupta, 2013; Sano and Williams, 1996). A more natural rate of ~10% assimilation (averaged from assimilation calculations based on CO_2 outflux estimates at Merapi, Vesuvius, Etna and Popocatepetl; Burton et al., 2013; Caliro et al., 2014; Frondini et al., 2004 and their averaged magma flux rate; Harris et al., 2011; Roberge et al., 2009; Rosi et al., 1987; Siswowidjoyo et al., 1995) is still a significant contribution across Earth ($\leq 5.5 \times 10^{14}$ g/y CO_2) suggesting crustal carbon could have played a significant role in the hotter climactic conditions at that time.

5. Concluding remarks

For continental volcanoes overlying carbonate strata, such as Popocatepetl, Merapi, Vesuvius, and Etna, carbonate–magma interaction within the upper plate must be considered when analyzing the erupted products. By observing basalt–calcite reaction experimentally, we better constrain both the phases and compositions expected at the wall rock–intrusion interface as well as the residual melt and gas that may be extruded at these vents. Our study shows that depth and temperature have opposing effects on the extent of carbonate assimilation and thus similar extent of assimilation may be realized over a wide range of conditions, i.e., from shallow and cooler to deep and hotter intrusions in the crust. Our study also indicates that limestone consumption by a basalt not only increases clinopyroxene production and shifts clinopyroxene stability to higher temperatures (>1200 °C with calcite versus <1200 °C without calcite, 1.0 GPa), but also makes residual clinopyroxene CaTs-rich. Calcite breakdown elevates CaO contents in the melt to extreme levels ($\leq$43.7 wt.%, volatile-free). Ultracalcic (CaO > 13.5 wt.%, $CaO/Al_2O_3 \gg 1.0$) melts are generated at moderate temperatures and pressures ($\geq$1175 °C, 1.0 GPa; $\geq$1150 °C, 0.8 GPa; $\leq$1100 °C, 0.5 GPa), suggesting the lower crustal contribution to ultracalcic melt inclusions may also be realized by moderate assimilation of carbonates rather than melting of clinopyroxenite.

The other notable contribution of calcite assimilation is release of CO_2-rich fluid, incurring the formation of scapolite over plagioclase in our experimental phase assemblages at higher temperatures. As a result of extreme calcite consumption ($\leq$~48%), the congestion of CO_2 in the closed system of these experiments may be the limiting factor for further assimilation. However, if the CO_2-rich vapor phase is vented and CaO-rich liquid expelled (an open system), new reaction surfaces may be created, which should lead to further assimilation. In this investigation, we were able to estimate a maximum of 2.1×10^9 to 2.1×10^{13} g/y CO_2 added to a typical arc volcanic system (10^{10}–10^{14} g/y magma flux, Crisp, 1984; White et al., 2006) at ~15 km solely from crustal decarbonation, which represents $\leq$7.7% of the present-day estimated total arc CO_2 flux. At this depth, a minimum of 6% (Popocatepetl, 1200 °C) and maximum of 92% (Etna, 1100 °C) of the magmatic flux at currently assimilating volcanoes (Merapi, Vesuvius, Etna or Popocatepetl) needs to react with calcite to provide enough excess CO_2 to match their present day emissions. Therefore, based on these 4 volcanoes, $\leq$3% of the current global CO_2 volcanic arc output may be crustally-derived. As such, it does not seem unlikely that extrapolating to several carbonate-assimilating systems could provide a significant source of exogenic carbon emission. Over the course of millennia, the combined product of numerous continental arc volcanoes intruding through crustal carbonates could elevate the atmospheric CO_2 content (Ganino and Arndt, 2009) by a maximum of 5.6×10^{15} g/y CO_2 (or $\leq 5.5 \times 10^{14}$ g/y CO_2 if the assimilation extent and magma flux is similar to current systems) during, for example, the late Cretaceous to early Paleogene, and ultimately affect long-term climate change (Lee et al., 2013). However, significant excess-CO_2 release by carbonate assimilation would imply

that a large proportion of arc magmas, either erupted or crystallized at depths, be silica-poor and ultracalcic in composition.

Acknowledgements

We gratefully acknowledge thorough and constructive reviews by Tobias Fischer, Silvio Mollo, and Giada Iacono-Marziano. This work received support from US NSF grant OCE 1338842 and Sloan Foundation (Deep Carbon Observatory) officer grant B2013-25 to RD.

Appendix A. Supplementary material

Supplementary material related to this article can be found online at http://dx.doi.org/10.1016/j.epsl.2015.06.053.

References

Aitken, B.G., 1983. T-X_{CO_2} stability relations and phase equilibria of a calcic carbonate scapolite. Geochim. Cosmochim. Acta 47, 351–362.

Balta, J.B., Beckett, J.R., Asimow, P.D., 2011. Thermodynamic properties of alloys of gold-74/palladium-26 with variable amounts of iron and the use of Au–Pd–Fe alloys as containers for experimental petrology. Am. Mineral. 96, 1467–1474. http://dx.doi.org/10.2138/am.2011.3637.

Barnes, C.G., Prestvik, T., Sundvoll, B., Surratt, D., 2005. Pervasive assimilation of carbonate and silicate rocks in the Hortavaer igneous complex, north-central Norway. Lithos 80, 179–199.

Barr, J.A., Grove, T.L., 2010. AuPdFe ternary solution model and applications to understanding the fO_2 of hydrous, high-pressure experiments. Contrib. Mineral. Petrol. 160, 631–643. http://dx.doi.org/10.1007/s00410-010-0497-z.

Behn, M.D., Kelemen, P.B., Hirth, G., Hacker, B.R., Massonne, H.-J., 2011. Diapirs as the source of the sediment signature in arc lavas. Nat. Geosci. 4, 641–646. http://dx.doi.org/10.1038/ngeo1214.

Burton, M.R., Sawyer, G.M., Granieri, D., 2013. Deep carbon emissions from volcanoes. Rev. Mineral. Geochem. 75, 323–354. http://dx.doi.org/10.2138/rmg.2013.75.11.

Caliro, S., Chiodini, G., Avino, R., Cardellini, C., Frondini, F., 2005. Volcanic degassing at Somma–Vesuvio (Italy) inferred by chemical and isotopic signatures of groundwater. Appl. Geochem. 20, 1060–1076. http://dx.doi.org/10.1016/j.apgeochem.2005.02.002.

Caliro, S., Chiodini, G., Paonita, a., 2014. Geochemical evidences of magma dynamics at Campi Flegrei (Italy). Geochim. Cosmochim. Acta 132, 1–15. http://dx.doi.org/10.1016/j.gca.2014.01.021.

Chadwick, J.P., Troll, V.R., Morgan, D., Gertisser, R., Waight, T.E., Davidson, J.P., Ginibre, C., 2007. Carbonate assimilation at Merapi Volcano, Java, Indonesia: insights from crystal isotope stratigraphy. J. Petrol. 48, 1793–1812. http://dx.doi.org/10.1093/petrology/egm038.

Conte, A.M., Dolfi, D., Gaeta, M., Misiti, V., Mollo, S., Perinelli, C., 2009. Experimental constraints on evolution of leucite-basanite magma at 1 and 10^{-4} GPa: implications for parental compositions of Roman high-potassium magmas. Eur. J. Mineral. 21, 763–782. http://dx.doi.org/10.1127/0935-1221/2009/0021-1934.

Crisp, J.A., 1984. Rates of magma emplacement and volcanic output. J. Volcanol. Geotherm. Res. 20, 177–211.

Dasgupta, R., 2013. Ingassing, storage, and outgassing of terrestrial carbon through geologic time. Rev. Mineral. Geochem. 75, 183–229. http://dx.doi.org/10.2138/rmg.2013.75.7.

Dasgupta, R., Mallik, A., Tsuno, K., Withers, A.C., Hirth, G., Hirschmann, M.M., 2013. Carbon-dioxide-rich silicate melt in the Earth's upper mantle. Nature 493, 211–215. http://dx.doi.org/10.1038/nature11731.

DeCelles, P.G., Ducea, M.N., Kapp, P., Zandt, G., 2009. Cyclicity in Cordilleran orogenic systems. Nat. Geosci. 2, 251–257. http://dx.doi.org/10.1038/ngeo469.

Deegan, F.M., Troll, V.R., Freda, C., Misiti, V., Chadwick, J.P., McLeod, C.L., Davidson, J.P., 2010. Magma–carbonate interaction processes and associated CO_2 release at Merapi Volcano, Indonesia: insights from experimental petrology. J. Petrol. 51, 1027–1051. http://dx.doi.org/10.1093/petrology/egq010.

Di Rocco, T., Freda, C., Gaeta, M., Mollo, S., Dallai, L., 2012. Magma chambers emplaced in carbonate substrate: petrogenesis of skarn and cumulate rocks and implications for CO_2 degassing in volcanic areas. J. Petrol. 53, 2307–2332. http://dx.doi.org/10.1093/petrology/egs051.

Duncan, M.S., Dasgupta, R., 2014. CO_2 solubility and speciation in rhyolitic sediment partial melts at 1.5–3 GPa – implications for carbon flux in subduction zones. Geochim. Cosmochim. Acta 124, 328–347. http://dx.doi.org/10.1016/j.gca.2013.09.026.

Duncan, M.S., Dasgupta, R., 2015. Pressure and temperature dependence of CO_2 solubility in hydrous rhyolitic melt: implications for carbon transfer to mantle source of volcanic arcs via partial melt of subducting crustal lithologies. Contrib. Mineral. Petrol. 169, 54. http://dx.doi.org/10.1007/s00410-015-1144-5.

Einaudi, M., Burt, D., 1982. A special issue devoted to skarn deposits: introduction-terminology, classification, and composition of skarn deposits. Econ. Geol. 77, 745–754.

Evans, B.W., Shaw, D.M., Haughton, D.R., 1969. Scapolite stoichiometry. Contrib. Mineral. Petrol. 24, 293–305. http://dx.doi.org/10.1007/BF00371272.

Freda, C., Gaeta, M., Karner, D.B., Marra, F., Renne, P.R., Taddeucci, J., Scarlato, P., Christensen, J.N., Dallai, L., 2006. Eruptive history and petrologic evolution of the Albano multiple maar (Alban Hills, Central Italy). Bull. Volcanol. 68, 567–591. http://dx.doi.org/10.1007/s00445-005-0033-6.

Freda, C., Gaeta, M., Misiti, V., Mollo, S., Dolfi, D., Scarlato, P., 2008. Magma–carbonate interaction: an experimental study on ultrapotassic rocks from Alban Hills (Central Italy). Lithos 101, 397–415. http://dx.doi.org/10.1016/j.lithos.2007.08.008.

Freda, C., Gaeta, M., Palladino, D.M., Trigila, R., 1997. The Villa Senni Eruption (Alban Hills, central Italy): the role of H_2O and CO_2 on the magma chamber evolution and on the eruptive scenario. J. Volcanol. Geotherm. Res. 78, 103–120. http://dx.doi.org/10.1016/S0377-0273(97)00007-3.

Frondini, F., Chiodini, G., Caliro, S., Cardellini, C., Granieri, D., Ventura, G., 2004. Diffuse CO_2 degassing at Vesuvio, Italy. Bull. Volcanol. 66, 642–651. http://dx.doi.org/10.1007/s00445-004-0346-x.

Gaeta, M., Di Rocco, T., Freda, C., 2009. Carbonate assimilation in open magmatic systems: the role of melt-bearing skarns and cumulate-forming processes. J. Petrol. 50, 361–385. http://dx.doi.org/10.1093/petrology/egp002.

Gaeta, M., Freda, C., Christensen, J.N., Dallai, L., Marra, F., Karner, D.B., Scarlato, P., 2006. Time-dependent geochemistry of clinopyroxene from the Alban Hills (Central Italy): clues to the source and evolution of ultrapotassic magmas. Lithos 86, 330–346. http://dx.doi.org/10.1016/j.lithos.2005.05.010.

Ganino, C., Arndt, N.T., 2009. Climate changes caused by degassing of sediments during the emplacement of large igneous provinces. Geology 37, 323–326. http://dx.doi.org/10.1130/G25325A.1.

Goff, F., Love, S.P., Warren, R.G., Counce, D., Obenholzner, J., Siebe, C., Schmidt, S.C., 2001. Passive infrared remote sensing evidence for large, intermittent CO_2 emissions at Popocatepetl. Chem. Geol. 177, 133–156.

Green, D.H., Schmidt, M.W., Hibberson, W.O., 2004. Island-arc ankaramites: primitive melts from fluxed refractory lherzolitic mantle. J. Petrol. 45, 391–403. http://dx.doi.org/10.1093/petrology/egg101.

Guffanti, M., Weaver, C.S., 1988. Distribution of Late Cenozoic volcanic vents in the Cascade range: volcanic arc segmentation and regional tectonic considerations. J. Geophys. Res. 93, 6513. http://dx.doi.org/10.1029/JB093iB06p06513.

Halldórsson, S.a., Hilton, D.R., Troll, V.R., Fischer, T.P., 2013. Resolving volatile sources along the western Sunda arc, Indonesia. Chem. Geol. 339, 263–282. http://dx.doi.org/10.1016/j.chemgeo.2012.09.042.

Harris, A., Steffke, A., Calvari, S., Spampinato, L., 2011. Thirty years of satellite-derived lava discharge rates at Etna: implications for steady volumetric output. J. Geophys. Res. 116, B08204. http://dx.doi.org/10.1029/2011JB008237.

Iacono-Marziano, G., Gaillard, F., Pichavant, M., 2007. Limestone assimilation and the origin of CO_2 emissions at the Alban Hills (Central Italy): constraints from experimental petrology. J. Volcanol. Geotherm. Res. 166, 91–105. http://dx.doi.org/10.1016/j.jvolgeores.2007.07.001.

Iacono-Marziano, G., Gaillard, F., Pichavant, M., 2008. Limestone assimilation by basaltic magmas: an experimental re-assessment and application to Italian volcanoes. Contrib. Mineral. Petrol. 155, 719–738. http://dx.doi.org/10.1007/s00410-007-0267-8.

Iacono-Marziano, G., Gaillard, F., Scaillet, B., Pichavant, M., Chiodini, G., 2009. Role of non-mantle CO_2 in the dynamics of volcano degassing: the Mount Vesuvius example. Geology 37, 319–322. http://dx.doi.org/10.1130/G25446A.1.

Jolis, E.M., Freda, C., Troll, V.R., Deegan, F.M., Blythe, L.S., McLeod, C.L., Davidson, J.P., 2013. Experimental simulation of magma–carbonate interaction beneath Mt. Vesuvius, Italy. Contrib. Mineral. Petrol. 166, 1335–1353. http://dx.doi.org/10.1007/s00410-013-0931-0.

Kerrick, D., 1977. The genesis of zoned skarns in the Sierra Nevada, California. J. Petrol. 18, 144–181.

Kogiso, T., Hirschmann, M.M., 2001. Experimental study of clinopyroxenite partial melting and the origin of ultra-calcic melt inclusions. Contrib. Mineral. Petrol. 142, 347–360. http://dx.doi.org/10.1007/s004100100295.

Kuhn, B., 2005. Scapolite Stability: Phase Relations and Chemistry of Impure Metacarbonate Rocks in the Central Alps. Swiss Federal Institute of Technology Zurich.

Lackey, J.S., Valley, J.W., Saleeby, J.B., 2005. Supracrustal input to magmas in the deep crust of Sierra Nevada batholith: evidence from high-$\delta^{18}O$ zircon. Earth Planet. Sci. Lett. 235, 315–330. http://dx.doi.org/10.1016/j.epsl.2005.04.003.

Lee, C.-T.a., Shen, B., Slotnick, B.S., Liao, K., Dickens, G.R., Yokoyama, Y., Lenardic, A., Dasgupta, R., Jellinek, M., Lackey, J.S., Schneider, T., Tice, M.M., 2013. Continental arc-island arc fluctuations, growth of crustal carbonates, and long-term climate change. Geosphere 9, 21–36. http://dx.doi.org/10.1130/GES00822.1.

Lehnert, K., Su, Y., Langmuir, C.H., Sarbas, B., Nohl, U., 2000. A global geochemical database structure for rocks. Geochem. Geophys. Geosyst. 1. http://dx.doi.org/10.1029/1999GC000026.

Marchev, P., Georgiev, S., Zajacz, Z., Manetti, P., Raicheva, R., von Quadt, A., Tommasini, S., 2009. High-K ankaramitic melt inclusions and lavas in the

Upper Cretaceous Eastern Srednogorie continental arc, Bulgaria: implications for the genesis of arc shoshonites. Lithos 113, 228–245. http://dx.doi.org/10.1016/j.lithos.2009.03.014.

Medard, E., 2006. Melting of amphibole-bearing wehrlites: an experimental study on the origin of ultra-calcic nepheline-normative melts. J. Petrol. 47, 481–504. http://dx.doi.org/10.1093/petrology/egi083.

Medard, E., Schmidt, M.W., Schiano, P., 2004. Liquidus surfaces of ultracalcic primitive melts: formation conditions and sources. Contrib. Mineral. Petrol. 148, 201–215. http://dx.doi.org/10.1007/s00410-004-0591-1.

Michaud, V., 1995. Crustal xenoliths in recent hawaiites from Mount Etna, Italy: evidence for alkali exchanges during magma–wall rock interaction. Chem. Geol. 122, 21–42. http://dx.doi.org/10.1016/0009-2541(94)00133-S.

Moecher, D., Essene, E., 1990. Phase equilibria for calcic scapolite, and implications of variable Al–Si disorder for P-T, T-X_{CO_2}, and a-X relations. J. Petrol. 31, 997–1024.

Moecher, D.P., Valley, J.W., Essene, E.J., 1994. Extraction and carbon isotope analysis of CO_2 from scapolite in deep crustal granulites and xenoliths. Geochim. Cosmochim. Acta 58, 959–967. http://dx.doi.org/10.1016/0016-7037(94)90518-5.

Mollo, S., Gaeta, M., Freda, C., Di Rocco, T., Misiti, V., Scarlato, P., 2010. Carbonate assimilation in magmas: a reappraisal based on experimental petrology. Lithos 114, 503–514. http://dx.doi.org/10.1016/j.lithos.2009.10.013.

Mollo, S., Vona, a., 2014. The geochemical evolution of clinopyroxene in the Roman Province: a window on decarbonation from wall-rocks to magma. Lithos 192–195, 1–7. http://dx.doi.org/10.1016/j.lithos.2014.01.009.

Roberge, J., Delgado-Granados, H., Wallace, P.J., 2009. Mafic magma recharge supplies high CO_2 and SO_2 gas fluxes from Popocatepetl volcano, Mexico. Geology 37, 107–110. http://dx.doi.org/10.1130/G25242A.1.

Rosi, M., Santacroce, R., Sheridan, M.F., 1987. Volcanic hazard. In: Santacroce, R. (Ed.), Quaderni de "La Ricerca Scientifica": Somma–Vesuvius. CNR, Roma, pp. 197–220.

Sano, Y., Williams, S.N., 1996. Fluxes of mantle and subducted carbon along convergent plate boundaries. Geophys. Res. Lett. 23, 2749–2752.

Schiano, P., Eiler, J.M., Hutcheon, I.D., Stolper, E.M., 2000. Primitive CaO-rich, silica-undersaturated melts in island arcs: evidence for the involvement of clinopyroxene-rich lithologies in the petrogenesis of arc magmas. Geochem. Geophys. Geosyst. 1, 1–33. http://dx.doi.org/10.1029/1999GC000032.

Schmidt, M.W., Green, D.H., Hibberson, W.O., 2004. Ultra-calcic magmas generated from Ca-depleted mantle: an experimental study on the origin of ankaramites. J. Petrol. 45, 531–554. http://dx.doi.org/10.1093/petrology/egg093.

Shaw, A.M., Hilton, D.R., Fischer, T.P., Walker, J.a., Alvarado, G.E., 2003. Contrasting He–C relationships in Nicaragua and Costa Rica: insights into C cycling through subduction zones. Earth Planet. Sci. Lett. 214, 499–513. http://dx.doi.org/10.1016/S0012-821X(03)00401-1.

Shaw, D.M., 1960. The geochemistry of scapolite Part I. Previous work and general mineralogy. J. Petrol. 1, 218–260. http://dx.doi.org/10.1093/petrology/1.1.218.

Sigurdsson, I., Steinthorsson, S., Grönvold, K., 2000. Calcium-rich melt inclusions in Cr-spinels from Borgarhraun, northern Iceland. Earth Planet. Sci. Lett. 183, 15–26.

Siswowidjoyo, S., Suryo, I., Yokoyama, I., 1995. Magma eruption rates of Merapi volcano, Central Java, Indonesia during one century (1890–1992). Bull. Volcanol. 57, 111–116.

Skora, S., Blundy, J.D., Brooker, R.A., Green, E.C.R., de Hoog, J.C.M., Connolly, J.A.D., 2015. Hydrous phase relations and trace element partitioning behaviour in calcareous sediments at subduction-zone conditions. J. Petrol. 56, 953–980.

Sorbadere, F., Médard, E., Laporte, D., Schiano, P., 2013. Experimental melting of hydrous peridotite–pyroxenite mixed sources: constraints on the genesis of silica-undersaturated magmas beneath volcanic arcs. Earth Planet. Sci. Lett. 384, 42–56. http://dx.doi.org/10.1016/j.epsl.2013.09.026.

Spandler, C., Martin, L., Pettke, T., 2012. Carbonate assimilation during magma evolution at Nisyros (Greece), South Aegean Arc: evidence from clinopyroxenite xenoliths. Lithos 146–147, 18–33. http://dx.doi.org/10.1016/j.lithos.2012.04.029.

Toutain, J.P., Sortino, F., Baubron, J.C., Richon, P., Surono, Sumarti, S., Nonell, A., 2009. Structure and CO_2 budget of Merapi volcano during inter-eruptive periods. Bull. Volcanol. 71, 815–826. http://dx.doi.org/10.1007/s00445-009-0266-x.

Troll, V.R., Hilton, D.R., Jolis, E.M., Chadwick, J.P., Blythe, L.S., Deegan, F.M., Schwarzkopf, L.M., Zimmer, M., 2012. Crustal CO_2 liberation during the 2006 eruption and earthquake events at Merapi volcano, Indonesia. Geophys. Res. Lett. 39. http://dx.doi.org/10.1029/2012GL051307.

Tsuno, K., Dasgupta, R., 2011. Melting phase relation of nominally anhydrous, carbonated pelitic-eclogite at 2.5–3.0 GPa and deep cycling of sedimentary carbon. Contrib. Mineral. Petrol. 161, 743–763. http://dx.doi.org/10.1007/s00410-010-0560-9.

Tsuno, K., Dasgupta, R., 2012. The effect of carbonates on near-solidus melting of pelite at 3 GPa: relative efficiency of H_2O and CO_2 subduction. Earth Planet. Sci. Lett. 319–320, 185–196. http://dx.doi.org/10.1016/j.epsl.2011.12.007.

Tsuno, K., Dasgupta, R., Danielson, L., Righter, K., 2012. Flux of carbonate melt from deeply subducted pelitic sediments – geophysical and geochemical implications for the source of Central American volcanic arc. Geophys. Res. Lett. 37, L16307. http://dx.doi.org/10.1029/2012GL052606.

Wallace, P.J., 2005. Volatiles in subduction zone magmas: concentrations and fluxes based on melt inclusion and volcanic gas data. J. Volcanol. Geotherm. Res. 140, 217–240. http://dx.doi.org/10.1016/j.jvolgeores.2004.07.023.

Watkinson, D., Wyllie, P., 1964. The limestone assimilation hypothesis. Nature 204, 1053–1054.

White, S.M., Crisp, J.a., Spera, F.J., 2006. Long-term volumetric eruption rates and magma budgets. Geochem. Geophys. Geosyst. 7, Q03010. http://dx.doi.org/10.1029/2005GC001002.